Mechanistic Features of the Sonochemical Degradation of Organic Pollutants

Thirugnanasambandam Sivasankar and Vijayanand S. Moholkar
Dept. of Chemical Engineering, Indian Institute of Technology Guwahati, Guwahati 781 039, Assam, India

DOI 10.1002/aic.11550
Published online June 18, 2008 in Wiley InterScience (www.interscience.wiley.com).

This work considers the mechanistic features of sonochemical degradation of volatile (chlorobenzene) and nonvolatile (phenol) organic pollutants. The sonochemical degradation of pollutant occurs in two pathways: thermal pyrolysis and hydroxylation. By coupling experimental results to bubble dynamics model, we have tried to establish relative contribution of these pathways to degradation of two kinds of pollutants. It is revealed that degradation of volatile pollutants occurs primarily by thermal pyrolysis while hydroxylation is the predominant mechanism of degradation of nonvolatile pollutants. The simulation results also help explain some interesting trends observed in degradation with reaction parameters such as initial pollutant concentration and salt addition to solution. These parameters are found to influence both pathways of degradation that leads to enhancement in degradation. However, the extent of this influence on hydroxylation and pyrolysis pathways is different for phenol and chlorobenzene. This is attributed to different partitioning behavior and solubility of the two pollutants.
 AIChE J, 54: 2206–2219, 2008
Keywords: sonochemistry, cavitation, bubble dynamics, wastewater treatment

Introduction

The toxic organic pollutants contributed by industrial wastewater and agricultural runoffs are complex refractory molecules, which are not easily degraded by the conventional methods.[1–3] Therefore, search for more efficient technologies is necessary for the degradation of such compounds. Development of the novel treatment methods encompasses investigation of advanced oxidation processes, which are characterized by production of hydroxyl radical ($OH^{\bullet}$) as the primary oxidant. Harnessing cavitation and sonochemistry as an advanced oxidation technology is being increasingly attempted in recent years.[4–20] Cavitation can be defined as nucleation, growth, and collapse of gas or vapor bubbles in liquid driven by the variation in the bulk liquid pressure due to passage of an ultrasound wave. As a result of cavitation bubble implosion, extremes of temperatures and pressures are generated at the center of collapsing bubble (~5000 K and ~500 bars).[21,22] The extreme conditions are short lived but have shown to result in the generation of highly reactive species such as hydroxyl ($OH^{\bullet}$), hydrogen ($H^{\bullet}$) and hydroperoxyl ($HOO^{\bullet}$) radicals and hydrogen peroxide.[23–25] As the bubble fragments during collapse, these radicals get mixed with the bulk liquid, where they can initiate and promote the hydroxylation reactions leading to degradation of pollutants.[26,27] Another possible mechanism for the degradation of pollutants is the thermal pyrolysis in the cavitation bubble. During the expansion phase of radial bubble motion, evaporation of the pollutant molecules occurs at the bubble wall and these molecules diffuse towards the center of the bubble. In the subsequent compression phase, the pollutant molecules diffuse outward, i.e. towards bubble wall, and condense at bubble wall. During the final moments of compression phase, the bubble motion becomes extremely rapid and not all of the pollutant molecules that have entered the bubble can condense. The entrapped molecules are subjected to extreme conditions generated during transient collapse and undergo

Correspondence concerning this article should be addressed to V. S. Moholkar at vmoholkar@iitg.ernet.in.

thermal pyrolysis.[28–30] The third possible mechanism for the hydrolysis of the organic pollutants is the formation of transient supercritical water packets in the close vicinity of cavitation bubble as proposed by Hua et al.[31] Out of these pathways, the major pathway contributing to the overall degradation depends on the nature and properties of the organic compound. An analysis of the degradation products of the pollutant provides a preliminary insight into the dominant chemical mechanism for the degradation. It can, nevertheless, be perceived that the radial motion of the cavitation bubble (or the bubble dynamics) driven by ultrasound wave is the physical basis of degradation of pollutants with irradiation of ultrasound.

In this study we have investigated the mechanistic aspects of the sonochemical degradation of the volatile and nonvolatile organic pollutants. Phenol and chlorobenzene have been selected as the model compounds in nonvolatile and volatile categories, respectively. These are very common pollutants found in industrial wastewater. In the last two decades several authors[6,29,32–40] have reported sonochemical degradation of phenol using ultrasound irradiation alone or in combination with various other techniques such as photocatalytic oxidation, Fenton's reagent oxidation, ozonation, peroxidation. The primary degradation products of phenol have been hydroquinone and catechol, which hint at attack of $OH^{\bullet}$ radical on phenol as the degradation pathway (or the principal chemical mechanism), which results in hydroxylated products. Sonochemical degradation of chlorobenzene has also been studied by many authors.[41–51] The degradation kinetics of chlorobenzene is found to be first order with major degradation products such as methane, acetylene, butenyne, butadiene, HCl, HOCl and $Cl^{\bullet}$ etc. These products hint at thermal pyrolysis as the principal chemical mechanism for the degradation. However, the approach in these studies for both compounds was mainly experimental and no confirmation of the degradation mechanism was made on the basis of a model for the radial motion of cavitation bubbles.

The principal aim of the present study is to provide a physical insight into the sonochemical degradation of the organic pollutants, which will decipher its primary physical mechanism. The principal physical phenomenon underlying the sonochemical degradation of the pollutants is radial motion of cavitation bubbles (or cavitation bubble dynamics). Therefore, any attempt to elucidate the physical mechanism of the process should basically mean establishing relationship between the sonochemical degradation through two pathways (viz. pyrolysis and hydroxylation) and the cavitation bubble dynamics. Therefore in this study we try to correlate the extent of degradation of the two pollutants under similar conditions to the physical properties of the pollutants and the fundamental phenomena of transport of vapor of water and organic pollutant across cavitation bubble using a bubble dynamics model that takes into account essential physics and chemistry of cavitation bubbles. Moreover, the influence of parameters such as initial concentration of pollutants and salt addition to the pollutant solution on the degradation kinetics is also explored from a mechanistic perspective. The results of this study not only establish the predominant physical mechanism for the sonochemical degradation of volatile and nonvolatile organic pollutants but also give an interesting account of the interlinks between cavitation physics and the chemistry of the sonochemical degradation of these pollutants.

Experimental

Reagents

Phenol (Merck, Grade: Synthesis), Chlorobenzene (Merck, Grade: GR), Sodium Chloride (Merck, Grade: Pure), Acetonitrile (Merck, Grade: HPLC) and Water (Merck, Grade: HPLC) were used as received. Elix water from Millipore (Model: Elix 3) was used for preparing the solutions of the pollutants. Bulk concentration of phenol and chlorobenzene in the solution was varied as 50 and 100 ppm.

Experimental setup

A schematic diagram of the experimental setup used in the present study is shown in Figure 1. For the sonication of the aqueous solutions of pollutants, a microprocessor based and programmable ultrasound processor was used (Sonics & Materials Inc., Model VCX 500). This processor had a frequency of 20 kHz with maximum power output of 500 W. The ultrasound probe of the processor was fabricated from high-grade titanium alloy and had a tip diameter of 13 mm. The processor had variable power output control, which was set at 20% during experiments, resulting in net consumption of 100 W power during sonication. It needs to be mentioned that this value corresponds to the theoretical maximum ultrasound intensity. The actual value of ultrasound intensity in the medium was measured using calorimetry.[52] In addition, the processor had facility of automatic frequency tuning and amplitude compensation, which ensures constant power delivery to ultrasound probe irrespective of the changes occurring in liquid medium. Sonication of the pollutant solution was done in a jacketed glass reactor (dimensions: height, 120 mm; diameter, 50 mm; and jacket diameter, 62 mm) placed on a laboratory jack, which could be raised or lowered for exact positioning of the ultrasound probe tip in the solution.

Experimental procedure and method of analysis

The volume of the solution of pollutant used for sonication was 150 ml at an initial temperature of 25°C. The total reaction time was 90 min; however, in order to avoid significant rise in the temperature of the solution, the sonication was done in cycles of 15 min sonication—5 min silent period. In addition, cooling water was circulated through the jacket during sonication in order to maintain the temperature of the reaction medium constant. The temperature of the solution was monitored continuously during sonication with a digital thermometer. The rise in temperature of solution during the experiment was ~2°C. Because of small reaction volume (150 ml) and single source of ultrasound in the medium (in the form of sonicator probe), the equilibration of reaction system (or steady state) after onset of sonication is expected to be quite rapid. Therefore, the procedure of intermittent sonication adopted in this study is not expected to cause reduction in overall (or gross) degradation of pollutant obtained during total 90 min of sonication.

Experiments were done for two concentrations of phenol and chlorobenzene, viz. 50 and 100 ppm. These values are

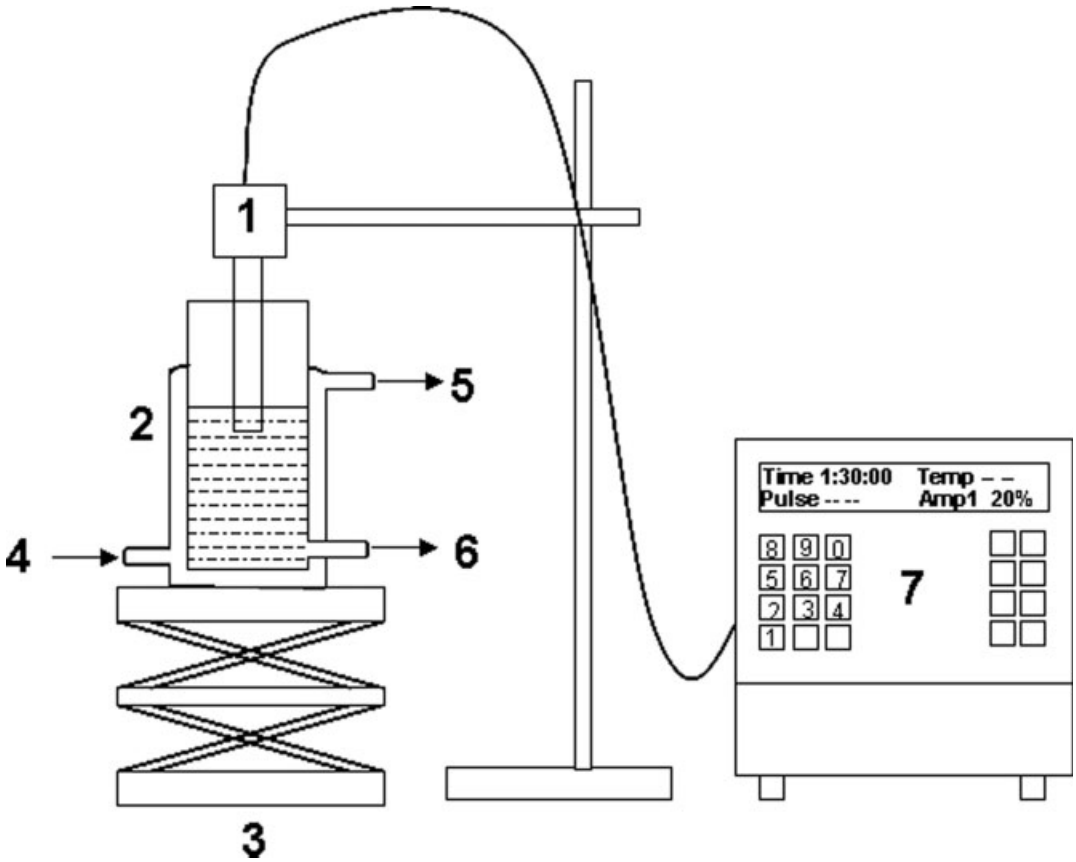

Figure 1. Experimental set-up.

[Legends: 1. Ultrasound probe; 2. Reactor with cooling jacket; 3. Laboratory jack; 4. Cooling water inlet; 5. Cooling water outlet; 6. Sample withdrawal port; 7. Control unit of the ultrasound processor].

typical of the concentration levels of the pollutants in industrial effluents.[53] For each of these concentrations, experiments were done for the pure solution and for the solution with 4% w/v (or 0.67 mol/l) salt addition. All experiments were done in triplicate to assess the reproducibity of the results. The mean of the degradation obtained in three experimental runs was taken into consideration for further analysis. We would like to mention that no gas was sparged through the reaction mixture during sonication. Therefore, the sonochemical reaction was left to the radicals generated out of cavitation bubbles already present in the medium—in the form of air pockets trapped in the solid boundaries such as tip of the ultrasound probe or the tiny air bubbles already suspended in the medium.

The final concentration of phenol and chlorobenzene in the solution after 90 min of sonication was determined using High Performance Liquid Chromatography (Perkin Elmer, Model: Series 200). A C18 column (Make: Chromatopak, dimensions: 250 $\times$ 4.6 mm, particle size of packing: 5 μm) was used and a mixture of acetonitrile:water (80:20) as the eluent. The flow rate of the eluent was maintained at 1 ml/min with the sample injection volume being 20 μl. The UV detector wavelengths for phenol and chlorobenzene were 275 and 205 nm respectively. We would like to categorically state that we have not made an analysis of the intermediate products of degradation of phenol and chlorobenzene, as these have been well studied and documented in previous literature (referred to in previous section). We have monitored the overall or gross degradation of the original pollutant in 90 min of sonication only and the analysis has been made on that basis.

The mathematical model

In the context of the present study, the problem of mathematical modeling comprises of simulating the radial motion of cavitation bubbles with the accompanying heat transfer and evaporation/entrapment of water and pollutant molecules, and finally determine the various chemical species that result out of transient collapse of the bubble. This subject has been an active area of research for the past three decades and various authors have dealt with the matter with different approaches.[27,30,54–63] The most general treatment of the problem of vapor transport in large amplitude nonlinear motion of the cavitation bubbles was presented by Storey and Szeri.[30] The principal result of analysis of Storey and Szeri[30] was that vapor transport in the bubble is a two-step process: diffusion to the bubble wall and condensation. Thus, it is influenced by relative magnitude of the bubble dynamics time scale (t_{osc}) with the time scales, viz. the time scale of vapor diffusion (t_{diff}) and the time scale of condensation (t_{cond}). In the final moments of bubble collapse, where the

bubble wall velocity reaches (or even exceeds) the velocity of sound in the medium, t_{osc} [dlt] t_{diff}, and the water vapor has insufficient time to diffuse to the bubble wall. Thus, it gets "trapped" or "frozen" in the cavitation bubble. Another mechanism which traps vapor in the cavitation bubble is the nonequilibrium phase change at the bubble wall. During the moments of transient collapse, t_{osc} [dlt] t_{cond} as well, and thus, the phase change at the bubble wall is nonequilibrium. This results in the entrapment of vapor molecules in the bubble. Evaluating the relative contribution of the two mechanisms to the overall vapor entrapment, Storey and Szeri[30] found that condition t_{osc} [dlt] t_{diff} is reached well before t_{osc}[dlt] t_{cond}. Thus, the diffusion of vapor plays a dominant role in the entrapment of the vapor in the cavitation bubble. In view of these conclusions, Toegel et al.[62] developed a diffusion-limited model using boundary layer approximation, which forms the framework for the model developed in the present study. Our bubble dynamics model makes two approximations as follows.

Analysis on Single Bubble Basis. We simulate the radial motion of the cavitation bubble in the bulk liquid medium using mathematical model for a single cavitation bubble. In other words, we ignore the influence of the bubble population in the neighborhood of a single bubble on its radial motion, and also the collective oscillations of bubble clouds in the medium. This approximation is based on the findings of Ilyichev et al.[64] who proved that all characteristic features of the cavitation bubble fields in the liquid medium can be explained on the basis of dynamic behavior of a single bubble. Moreover, other studies (Prasad Naidu et al.,[54] Sivasankar et al.[52]) using a model reaction (oxidation of KI to liberate iodine) have also proven that the trends in the yield of a sonochemical reaction can be explained on the basis of simulations of radial motion of a single cavitation bubble. This further supports our approach.

Thermodynamic Equilibrium of the Bubble Contents. While calculating the composition of the bubble contents at the moment of transient collapse, we assume that equilibrium is attained among various chemical species present in the bubble. Moreover, in the energy balance for the bubble we do not incorporate various radical reactions along with their heats of reactions. It needs to be mentioned that the endothermicity of some of the reactions (for example $H_2O \rightleftharpoons H^{\bullet} + OH^{\bullet}$) works towards reduction in the temperature peak attained during transient bubble collapse. The assumption of attainment of thermodynamic equilibrium at the bubble collapse is based on the relative magnitudes of the bubble collapse time scale and the time scales of various radical reactions. The time scale of bubble collapse, as determined by Storey and Szeri[30] is of the order of few tens of nanoseconds ($\sim 10^{-8}$). The specific rate constants for the various radical reactions calculated from the Arrhenius equation at temperatures 2500–3000 K (typical of the temperature peaks attained during transient bubble collapse) are of the order of 10^{12} cm^3 mol^{-1} s^{-1}. Moreover, the concentrations of various species in the bubble at the moment of collapse are very high. An order of magnitude calculation done with representative numbers [$\sim 10^{10}$ molecules or 10^{-13} moles in a 10 μm bubble (or $\sim 10^{-4}$ cm) compressed to 1/10th of its original size, i.e. $\sim 10^{-5}$ cm] puts concentrations as high as $\sim$100 mol/cm^3. As a collective result of these two features, rates of various reactions among various species present in the bubble are expected to be extremely fast. Even with a conservative estimate of concentration, the time-scale for the reaction (t_{react}) can be taken as $\sim$1/specific reaction rate. Comparison of the time scale of bubble collapse with the time scale of reactions reveals that the latter is at least two orders of magnitude smaller. Thus, thermodynamic equilibrium should prevail till the point of minimum radius during collapse. This justifies our assumption of thermodynamic equilibrium. Brenner et al.[26] have also supported the attainment of thermal equilibrium in a sonoluminescing bubble.

We emphasize that our approach with the above approximations addresses the basic physics of the problem, which is sufficient for the present case. A more rigorous approach relaxing approximations in this study would only modify quantitative answers.

Radial motion of bubble

The radial motion of the bubble is described by the Keller-Miksis equation[65,66]:

$$\left(1-\frac{dR/dt}{c}\right)R\frac{d^2R}{dt^2}+\frac{3}{2}\left(1-\frac{dR/dt}{3c}\right)\left(\frac{dR}{dt}\right)^2 = \frac{1}{\rho_L}\left(1+\frac{dR/dt}{c}\right)(P_i-P_t)+\frac{R}{\rho_L c}\frac{dP_i}{dt}-4v\frac{dR/dt}{R}-\frac{2\sigma}{\rho_L R}. \quad (1)$$

This is a modification of the Rayleigh-Plesset equation, which takes into account liquid compressibility. R denotes the radius of the bubble at time t and ρ_L, σ, v denote the physical properties of the liquid medium, viz. the density, surface tension and kinematic viscosity respectively. c is the speed of sound in the medium and the pressure inside the bubble (P_i) is written using van der Waals type equation of state[67]:

$$P_i = \frac{N_{tot}(t)\ kT}{\left[\frac{4\pi}{3}\left(R^3(t)-h^3\right)\right]} \quad (2)$$

k is the Boltzmann constant, N_{tot} denotes the total number of molecules in the bubble that vary according to condensation/vaporization of the bulk medium (i.e. the solution containing the pollutant, in present case) and T is the temperature inside the bubble. h is the van der Waal's hard core radius of various species in the bubble viz. nitrogen, oxygen, water and chlorobenzene or phenol. As an approximation we take a common value $h\ R_0/8.86$ for all species, where R_0 is the equilibrium radius of bubble. A simple expression for P_t (the bulk pressure during ultrasound irradiation) is written as[67]:

$$P_t = P_0 - P_A \sin(2\pi f t) \quad (3)$$

here P_0 is the ambient pressure and P_A and f denote the pressure amplitude and frequency of acoustic wave.

Mass transfer across bubble

During the radial motion of bubble, both gas and water vapor diffuse across the bubble wall. The time scale for the diffusion of gas is $\sim {R_0}^2/D$ where D is the diffusion coeffi-

cient.[63] For representative values as $R_0 \sim 10$ μm, $D \sim 10^{-9}$ m^2/s, the time scale for the gas diffusion is 0.1 s, which is far higher than time scale of bubble dynamics[26] ($\sim$50 μs for 20 kHz ultrasound wave). Thus, the transport of gas across bubble can be ignored. Diffusion of vapor across the bubble wall, however, needs to be accounted for. In the present situation, the bulk liquid medium contains two components (either chlorobenzene-water or phenol-water) that evaporate into the bubble. The surface temperature of bubble exceeds the bulk water temperature only for a very brief moment during collapse.[55] On this basis, the present model divides the bubble into two parts[1]: a cold boundary layer in thermal equilibrium with liquid and[2] a hot homogeneous core. The rate of change of vapor molecules in the bubble is given by:

$$\frac{dN_w}{dt} = 4\pi R^2 D_w \left.\frac{\partial C_w}{\partial r}\right|_{r=R} \approx 4\pi R^2 D_w \left(\frac{C_{wR} - C_w}{l_{diff}}\right) \quad (4)$$

Pollutant (either chlorobenzene or phenol) vapor:

$$\frac{dN_p}{dt} = 4\pi R^2 D_p \left.\frac{\partial C_p}{\partial r}\right|_{r=R} \approx 4\pi R^2 D_p \left(\frac{C_{pR} - C_p}{l_{diff}}\right) \quad (5)$$

where l_{diff} is the instantaneous diffusive penetration depth and D_w and D_p are the effective diffusion coefficients for water vapor and pollutant respectively. Using dimensional analysis[62,63] it is taken to be $l_{diff} = \sqrt{D_w t_{osc}}$ for water molecules and $l_{diff} = \sqrt{D_p t_{osc}}$ for pollutant molecules. t_{osc} is the time scale of bubble dynamics estimated as $R/|dR/dt|$, again using dimensional analysis. C_{wR} and C_{pR} is the equilibrium concentration of the water and pollutant molecules at bubble wall. C_w and C_p are the concentrations of water and the pollutant in the core of the bubble. Since the concentrations of phenol and chlorobenzene are rather dilute, the behavior of solution is close to ideal and the activity coefficients of solvent and solute can be assumed to $\sim$1. Thus, we assume the Raoult's law to hold good. The total vapor pressure of the pollutant-water mixture in this situation is:

$$P_v = x_{wR} P_w + x_{pR} P_p \quad (6)$$

where x_{wR} and x_{pR} are the mole fractions of water and pollutant components in liquid. The concentrations of water and pollutant molecules at bubble-bulk interface are written in terms of their partial pressures:

$$C_{wR} = (x_{wR} P_w)/kT_0 \text{ and } C_{pR} = (x_{pR} P_p)/kT_0 \quad (7)$$

The mole fraction (or in other words, concentration) of the pollutant molecule at the bubble-water interfacial region is not the same as the bulk concentration of the pollutant in the medium (50 or 100 ppm). This is due to the fact that hydrophobic repulsive interactions of the pollutant molecules with aqueous phase drive the pollutant molecules towards the bubble-bulk interface.[68,69] As a result, the concentration of the pollutant molecules in the thin liquid shell surrounding the bubble increases. A direct measurement of the pollutant concentration in the interfacial region is beyond the capabilities of the instrumentation used in the present study. However, an indirect estimation of the interfacial concentration has been done by Bapat et al.[70] and Seymour and Gupta.[40]

The approach of Bapat et al.[70] was theoretical. Using the Gibb's equation for the surface excess of solute as basis,[71] they measured the reduction in the surface tension of the aqueous solution of phenol with concentration of phenol. Correlating the slope of the plot of surface tension vs. bulk concentration to the Gibb's equation, Bapat et al.[70] determined the surface excess of phenol for bulk concentration of 1 mol/m^3. Later, with simultaneous analysis of the surface concentration of phenol and water molecules at bubble-bulk interface, Bapat et al.[70] concluded that the concentration of phenol at bubble-bulk interface at equilibrium conditions would be 264 times the bulk concentration.

Seymour and Gupta[40] measured the partitioning behavior of chlorobenzene and phenol between an organic phase (diethyl ether) and water. A partition coefficient $K_{ether\text{-}water}$ was defined as c_{org}/c_{aq} where c_{org} is the concentration of pollutant in the organic phase and c_{aq} is the concentration in the aqueous phase. This partition coefficient was related to the interface-bulk liquid partition coefficient as:

$$K_{interface\text{-}bulk} = c_1 K_{ether\text{-}water} \quad (8)$$

where c_1 is constant of proportionality. With the best fit of experimental data, Seymour and Gupta found $c_1 = 4$ for chlorobenzene and $c_1 = 0.67$ for phenol. Additional of salt (NaCl) to the aqueous phase raises the ionic strength of the solution, and hence, the hydrophobic repulsive interactions. Because of this, the pollutant molecules are driven to the organic phase to a greater extent, which results in a rise in c_{org} and $K_{interface\text{-}bulk}$. The values of partition coefficients for chlorobenzene and phenol are listed in Table 1.

The enrichment of phenol at bubble-bulk interface as determined by Seymour and Gupta[40] and Bapat et al.[70] differs by two orders of magnitude. However, attainment of equilibrium between bubble interface and bulk medium is difficult to achieve under transient cavitation conditions where bubble undergoes large-amplitude radial motion. The time scale of this motion is same as that of the ultrasound wave (50 μs for 20 kHz frequency). The time for the diffusion of phenol to the bubble interface through the boundary layer is expected to be several orders of magnitude higher. For representative values of boundary layer thickness around bubble as $\sim$1 μm and diffusion coefficient of pollutant in water as 10^{-10} m^2/s, the time scale of diffusion of phenol is $\sim$1 ms. Because of large difference in the time scale of diffusion of phenol and the time scale of radial motion of bubble, the bubble interface is not likely to attain equilibrium (as assumed by Bapat et al.[70]) under transient cavitation conditions. The enrichment factor determined empirically (under nonequilibrium conditions) by Seymour and Gupta,[40] thus, seems to be more practical. Therefore we have used the data of Seymour and Gupta[40] for our analysis.

Using the partition coefficients in Table 1, we estimate the mole fraction of the pollutant molecules in the interfacial region as:

$$x_{pR} = K_{interface\text{-}bulk} x_p \quad (9)$$

where x_p is the overall or bulk mole fraction of the pollutant in the medium. It must be mentioned that x_{pR} cannot rise indefinitely with addition of salt. The upper limit to x_{pR} is decided by the solubility of the pollutant, which is 0.5 g/l for

Table 1. Partitioning Behavior* (A) and Mole Fractions (B) of the Pollutants

(A) Partitioning Behavior

Phenol			Chlorobenzene		
Salt Concentration	$K_{\text{ether-water}}$	$K_{\text{interface-bulk}}$	Salt Concentration	$K_{\text{ether-water}}$	$K_{\text{interface-bulk}}$
0% w/v	4.9	3.283	0% w/v	7.3	29.2
4% w/v	17.5	11.725	4% w/v	12.0	48.0

(B) Mole Fractions

Concentration of Solution	Phenol	Chlorobenzene
	Overall or Bulk Mole Fraction (x_p)	
50 ppm solution	9.574×10^{-6}	7.995×10^{-6}
100 ppm solution	1.915×10^{-5}	1.6×10^{-6}
	Saturation Mole Fraction (x_s)	
	1.53×10^{-3}	8×10^{-5}

*Data taken from Seymour and Gupta.[40]

chlorobenzene and 8 g/l for phenol. Table 1 lists the values of bulk (x_p) and saturation (x_s) mole fraction of phenol and chlorobenzene. If (x_p $K_{\text{interface-bulk}}$) $>x_s$, the interface remains saturated with pollutant, i.e. $x_{pR} = x_s$.

P_w and P_p are the vapor pressures of water and pollutant in pure form at the bulk temperature (T_0). We use the following Antoine's equations for calculation of P_w and P_p (in Pa)[72]:

$$P_p(\text{for phenol}) = 10^5 \times 10^{(4.24688-1509.677/(T-98.949))} \quad (10)$$

$$P_p(\text{for chlorobenzene}) = 10^5 \times 10^{(4.11083-1435.675/(T-55.124))} \quad (11)$$

$$P_w = \frac{10^5}{760}\exp\left(18.3036 - \frac{3816.44}{T-46.13}\right). \quad (12)$$

The influence of salt addition to the solution on the vapor pressure of water is accounted for by the following equation[73]:

$$P'_w = P_w(1 - 0.537C_B) \quad (13)$$

Limits on diffusion length

At the instances of maximum and minimum radius, the bubble wall velocity is zero, and thus, an alternate expression is needed for diffusion length. We set this limit as R/π after identifying that vapor transport is governed by pure diffusion equation for condition $dR/dt = 0$. The limit R/π is set on the basis of solution of the diffusion equation in spherical geometry. For greater details on this, we refer the reader to our earlier papers.[74,75] Thus, the diffusion length for water molecules is: $l_{\text{diff}} = \min\left(\sqrt{\frac{RD_w}{|dR/dt|}}, \frac{R}{\pi}\right)$ while the diffusion length for the pollutant molecules is: $l_{\text{diff}} = \min\left(\sqrt{\frac{RD_p}{|dR/dt|}}, \frac{R}{\pi}\right)$.

Determination of diffusion coefficient

In the present situation (air bubbles oscillating in the aqueous solution of pollutants) we encounter a quaternary system: nitrogen-oxygen-water-pollutant. The diffusion of nitrogen and oxygen across bubble wall is ignored for the reasons stated earlier. For water and the pollutant (either phenol or chlorobenzene) we first calculate the binary diffusion coefficients using kinetic theory of gases[76] with properties of boundary layer evaluated at bulk temperature (for greater details we refer the reader to our earlier papers[74,75]). From these binary coefficients, the overall (or effective) diffusion coefficient for water (D_w) and the pollutant (D_p) is calculated as[77]:

$$\frac{1}{D_w} = \frac{\varepsilon_{N_2}}{(1-\varepsilon_w)D_{w-N_2}} + \frac{\varepsilon_{O_2}}{(1-\varepsilon_w)D_{w-O_2}} + \frac{\varepsilon_p}{(1-\varepsilon_w)D_{p-O_2}} \quad (14)$$

$$\frac{1}{D_p} = \frac{\varepsilon_{N_2}}{(1-\varepsilon_p)D_{p-N_2}} + \frac{\varepsilon_{O_2}}{(1-\varepsilon_p)D_{p-O_2}} + \frac{\varepsilon_w}{(1-\varepsilon_p)D_{p-H_2O}} \quad (15)$$

Here ε denotes the mole fraction of the individual component. Subscripts p, O_2, and N_2, w represent pollutant, oxygen, nitrogen, and water, respectively.

Heat transfer across bubble

In analogy with mass transfer, the rate of heat transfer (Q) across bubble wall is:

$$\frac{dQ}{dt} = 4\pi R^2 \lambda \left.\frac{\partial T}{\partial r}\right|_{r=R} \approx 4\pi R^2 \lambda \left(\frac{T_0 - T}{l_{\text{th}}}\right) \quad (16)$$

where λ is the effective thermal conductivity of bubble contents and l_{th} is the thermal diffusion length: $\min\left(\sqrt{\frac{R\kappa}{|dR/dt|}}, \frac{R}{\pi}\right)$. Thermal diffusivity ($\kappa$) is calculated as: $\kappa = \lambda/\rho_{\text{mix}}C_{p,\text{mix}}$, where ρ_{mix} and $C_{p,\text{mix}}$ represent the overall density and specific heat capacity of the mixture of various species in the bubble. The molecular specific heats (C_p) for various components are as follows:

$$N_2 = 7k/2,\ O_2 = 7k/2,\ \text{and } H_2O = 4k.$$

Since the concentration of pollutant in the solution is quite small, so will be the equilibrium pressure at the bubble-bulk interface and the diffusive flux of the pollutant. The bubble contents will be dominated by air and water vapor. In view

of this, we have not included the pollutant as a component in the determination of the thermal conductivity and thermal diffusivity. The thermal conductivity of the bubble contents has been calculated considering only three components, viz. oxygen, nitrogen, and water vapor. To calculate the effective thermal conductivity, we first determine the thermal conductivity (λ) and viscosity (η_i) of the individual species using the kinetic theory of gases (again we refer readers to our earlier papers[74,75] for greater details). The effective thermal conductivity of the mixture of species is given by following relation[78]:

$$\lambda_{\text{mix}} = \sum \frac{\varepsilon_i \lambda_i}{\sum \varepsilon_j \phi_{ij}} \tag{17}$$

where $i, j = O_2$, N_2, and H_2O, and

$$\phi_{ij} = \frac{1}{\sqrt{8}} \left(1 + \frac{m_i}{m_j}\right)^{-1/2} \left[1 + \left(\frac{\eta_i}{\eta_j}\right)^{-1/2} \left(\frac{m_i}{m_j}\right)^{1/4}\right]^2 \tag{18}$$

where m_i and m_j are the molecular masses of various species.

Overall energy balance

During the radial motion, the bubble is an open system through which water and pollutant molecules diffuse. However, in a very dilute solution (such as 50 and 100 ppm of organic pollutant), the transaction of water molecules through bubble wall will be several orders of magnitude larger than the solute or pollutant molecules. Thus, we write the energy balance for the bubble on the basis of ternary system: O_2-N_2-H_2O. The total energy balance for the bubble content is:

$$\frac{dE}{dt} = \frac{dQ}{dt} - \frac{dW}{dt} + h_w \frac{dN_w}{dt} \tag{19}$$

The total energy E is a function of temperature and volume of the bubble and the number of molecules of various species in it. The rate of change of E is:

$$\begin{aligned}\frac{dE}{dt} = &\left(\frac{\partial E}{\partial N_W}\right)_{N_{N_2}, N_{O_2}, V, T} \left(\frac{dN_W}{dt}\right) + \left(\frac{\partial E}{\partial N_{N_2}}\right)_{N_W, N_{O_2}, V, T} \left(\frac{dN_{N_2}}{dt}\right) \\ &+ \left(\frac{\partial E}{\partial N_{O_2}}\right)_{N_{N_2}, N_W, V, T} \left(\frac{dN_{O_2}}{dt}\right) + \left(\frac{\partial E}{\partial T}\right)_{N_W N_{N_2}, N_{O_2}, V} \left(\frac{dT}{dt}\right) \\ &+ \left(\frac{\partial E}{\partial V}\right)_{N_W, N_{N_2}, N_{O_2}, T} \left(\frac{dV}{dt}\right)\end{aligned} \tag{20}$$

where V is the volume of the bubble and N_{N_2}, N_{O_2}, and N_W are the number of nitrogen, oxygen and water molecules in the bubble. For the reasons stated earlier, we ignore the transport of oxygen and nitrogen molecules across bubble, and hence: $dN_{N_2}/dt = dN_{O_2}/dt = 0$. dN_W/dt is the rate of change of water vapor content of the bubble and is evaluated using Eq. 4. Moreover, we identify thermodynamic relations

$$\left(\frac{\partial E}{\partial T}\right)_{N_W, N_{N_2}, N_{O_2}, V} = C_{V,\text{mix}} \text{ and } \left(\frac{\partial E}{\partial V}\right)_{N_W, N_{N_2}, N_{O_2}, T} = 0 \tag{21}$$

as the internal energy of an ideal gas is a principal function of composition and temperature. The specific enthalpy of the water molecules entering the bubble from cold bubble interface is: $h_w = 4kT_0$. $(\partial E/\partial N_w)$ is the specific internal energy of water molecule (U_w) and is written as

$$\left(\frac{\partial E}{\partial N_w}\right) = U_w = N_w kT \left(3 + \sum_{i=1}^{3} \frac{\theta_i/T}{\exp(\theta_i/T) - 1}\right) \tag{22}$$

with characteristics vibration temperatures (θ_i) for water molecule are listed below. Equating the RHS of Eqs. 14 and 15 above we get:

$$C_{V,\text{mix}} \frac{dT}{dt} = \frac{dQ}{dt} - P_i dV + (h_w - U_w) \frac{dN_w}{dt} \tag{23}$$

The specific heat of mixture $C_{V,\text{mix}}$ is written in terms of the molecular specific heat of individual components ($C_{V,i}$) and the number of molecules of individual components (N_i) as:

$$C_{V,\text{mix}} = \sum C_{V,i} N_i \quad i = N_2 O_2 H_2 O \tag{24}$$

The molecular specific heats C_V for various components are written as:

$$C_{V,N_2} = k\left[\frac{5}{2} + \frac{(\theta_{N_2}/T)^2 \exp(\theta_{N_2}/T)}{(\exp(\theta_{N_2}/T) - 1)^2}\right] \quad \theta_{N_2} = 3350 \text{ K} \tag{25}$$

$$C_{V,O_2} = k\left[\frac{5}{2} + \frac{(\theta_{O_2}/T)^2 \exp(\theta_{O_2}/T)}{(\exp(\theta_{O_2}/T) - 1)^2}\right] \quad \theta_{O_2} = 2273 \text{ K} \tag{26}$$

$$C_{V,W} = k\left[3 + \sum_{i=1}^{3} \frac{(\theta_i/T)^2 \exp(\theta_i/T)}{(\exp(\theta_i/T) - 1)^2}\right] \quad \theta_{i,W} = 2295, 5255, 5400 \text{ K} \tag{27}$$

Numerical solution

Equations 1, 4, 5, 16, and 23 give the formulation of radial motion of bubble with accompanying heat and mass transfer. For the convenience of the reader we have summarized the complete bubble dynamics formulation in Table 2 along with boundary conditions. We use the Runge-Kutta 4th order-5th order method with adaptive step size[79] (also known as Cash-Karp method) for the numerical solution of these simultaneous ordinary differential equations. The collapse of the cavitation bubble depends on several factors such as surface instability, local flow conditions, and bubble population in the vicinity of the cavitation bubble. As a conservative estimate, the condition for the bubble collapse is taken to be first compression after an initial expansion. Four important parameters required for the simulation of the radial motion of the cavitation bubble are: (1) frequency and (2) pressure amplitude of ultrasound, (3) vapor pressure of water and pollutant and (4) initial (or equilibrium) bubble radius. Numerical values for these parameters have been determined as follows: The frequency of the wave (f) is taken as 20 kHz (i.e., the frequency of the ultrasound processor). The pressure amplitude of the acoustic wave (P_A) was determined as 1.5 bar using calorimetric techniques. However,

Table 2. Summarization of the Bubble Dynamics Formulation

Variable	Equation	Boundary Condition
1. Radius of the bubble (R)	$\left(1-\frac{dR/dt}{c}\right)R\frac{d^2R}{dt^2}+\frac{3}{2}\left(1-\frac{dR/dt}{3c}\right)\left(\frac{dR}{dt}\right)^2=\frac{1}{\rho_L}\left(1+\frac{dR/dt}{c}\right)\times(P_i-P_t)+\frac{R}{\rho_L c}\frac{dP_i}{dt}-4v\frac{dR/dt}{R}-\frac{2\sigma}{\rho_L R}$	At $t=0$, $R=R_o$ and $dR/dt=0$.
2. Bubble wall velocity (dR/dt)	Internal pressure in the bubble: $P_i=\frac{N_{tot}(t)kT}{\left[4\pi\left(R^3(t)-h^3\right)/3\right]}$ Pressure in bulk liquid medium: $P_t=P_0-P_A\sin(2\pi ft)$	
3. Number of water molecules in the bubble (N_w)	$\frac{dN_w}{dt}=4\pi R^2D_w\left.\frac{\partial C_w}{\partial r}\right\|_{r=R}\approx 4\pi R^2D_w\left(\frac{C_{wR}-C_w}{l_{diff}}\right)$	At $t=0$, $N_w=0$ and $N_p=0$
4. Number of pollutant molecules in the bubble (N_p)	$\frac{dN_p}{dt}=4\pi R^2D_p\left.\frac{\partial C_p}{\partial r}\right\|_{r=R}\approx 4\pi R^2D_p\left(\frac{C_{pR}-C_p}{l_{diff}}\right)$ Instantaneous diffusive penetration depths: $l_{diff}=\min\left(\sqrt{\frac{RD_w}{\lvert dR/dt\rvert}},\frac{R}{\pi}\right);\ l_{diff}=\min\left(\sqrt{\frac{RD_p}{\lvert dR/dt\rvert}},\frac{R}{\pi}\right)$ Diffusion coefficients: $\frac{1}{D_w}=\frac{\varepsilon_{N_2}}{(1-\varepsilon_w)D_{w-N_2}}+\frac{\varepsilon_{O_2}}{(1-\varepsilon_w)D_{w-O_2}}+\frac{\varepsilon_p}{(1-\varepsilon_w)D_{p-O_2}}$ $\frac{1}{D_p}=\frac{\varepsilon_{N_2}}{(1-\varepsilon_p)D_{p-N_2}}+\frac{\varepsilon_{O_2}}{(1-\varepsilon_p)D_{p-O_2}}+\frac{\varepsilon_w}{(1-\varepsilon_p)D_{p-H_2O}}$	At $t=0$, $Q=0$
5. Heat transfer through bubble (Q)	$\frac{dQ}{dt}=4\pi R^2\lambda\left.\frac{\partial T}{\partial r}\right\|_{r=R}\approx 4\pi R^2\lambda\left(\frac{T_0-T}{l_{th}}\right)$ Thermal diffusion length: $l_{th}=\min\left(\sqrt{\frac{R\kappa}{\lvert dR/dt\rvert}},\frac{R}{\pi}\right)$ Thermal conductivity: $\lambda_{mix}=\sum\frac{\varepsilon_i\lambda_i}{\sum\varepsilon_j\phi_{ij}}$ $\phi_{ij}=\left(1/\sqrt{8}\right)\left(1+m_i/m_j\right)^{-1/2}\left[1+\left(\eta_i/\eta_j\right)^{-1/2}\left(m_i/m_j\right)^{1/4}\right]^2$	
6. Temperature of the bubble (T)	$C_{V,mix}dT/dt=dQ/dt-P_idV+(h_w-U_w)dN_w/dt$ Mixture heat capacity: $C_{V,mix}=\sum C_{V,i}N_i$ Molecular properties of water: Enthalpy: $h_w=4kT_o$ Internal energy: $U_w=N_wkT\left(3+\sum_{i=1}^{3}\frac{\theta_i/T}{\exp(\theta_i/T)-1}\right)$	Initial condition: At $t=0$, $\boldsymbol{T}=\mathbf{To}$ (the temperature of bulk liquid).

the ultrasound wave undergoes attenuation during its passage through the medium. Therefore, the actual acoustic wave amplitude sensed by the bubble is lesser than that at the ultrasound probe tip. A direct measurement of this value is beyond the capabilities of instrumentation used in this study, and hence, we take a representative value as 1.25 bar, assuming ~15% attenuation. We would like to specifically mention that the attenuation of 15% is merely a representative number. Use of any other value (10 or 20%) makes only quantitative changes to the simulation results with the trends remaining essentially unchanged. The equilibrium radius of the bubble (R_0) is difficult to estimate. Moreover, the equilibrium size of the bubble keeps on changing due to phenomena such as rectified diffusion, fragmentation of the bubble, etc. We have chosen a representative value of R_0 as 10 μm for simulations. Once again we would like to mention that choice of any other value for this parameter (for example 5 or 15 μm) makes only quantitative changes to the simulation results with trends essentially remaining unchanged. The vapor pressure of water and pollutant has been calculated at the initial temperature of the bulk medium (i.e., 25°C) using Antoine equations (Eqs. 10–12). For the simulation of bubble motion in salt-added solution, we take into account the reduction in vapor pressure of water, as explained earlier (Eq. 13). However, changes in other physical

properties of water such as density, viscosity, surface tension and heat capacity have been neglected as the salt concentrations used in the experiment (4% w/v or 0.67 g/l) is too small to make any appreciable changes to the physical properties.[73]

The composition of the bubble at the time of collapse is calculated assuming that thermodynamic equilibrium is reached in the bubble. The equilibrium mole fraction of various species in bubble at the conditions of temperature and pressure at the first compression of the bubble was calculated using software FACTSAGE, which uses the free energy minimization algorithm proposed by Eriksson.[80] It should be noted that FACTSAGE gives an equilibrium distribution of the species resulting from transient collapse of the cavitation bubble. These species are formed out of dissociation of various molecules (gas, water vapor, and pollutant vapor) entrapped in the bubble at the moment of transient collapse. These are different than the degradation intermediates obtained with GC-MS or HPLC analysis of the samples withdrawn from the bulk medium. Some of the species resulting from the cavitation bubble are radicals, which can further react with pollutant molecules in the bulk giving variety of products (mentioned in the Introduction section), which are detected as degradation intermediates. The water vapor and pollutant molecules entrapped in the bubble are subjected to extreme conditions generated at the transient bubble collapse, which results in dissociation of water vapor into radical species and pyrolysis of the pollutant creating mineralization products. Therefore, the species obtained with FACTSAGE are expected to mainly comprise of radicals and mineralization products.

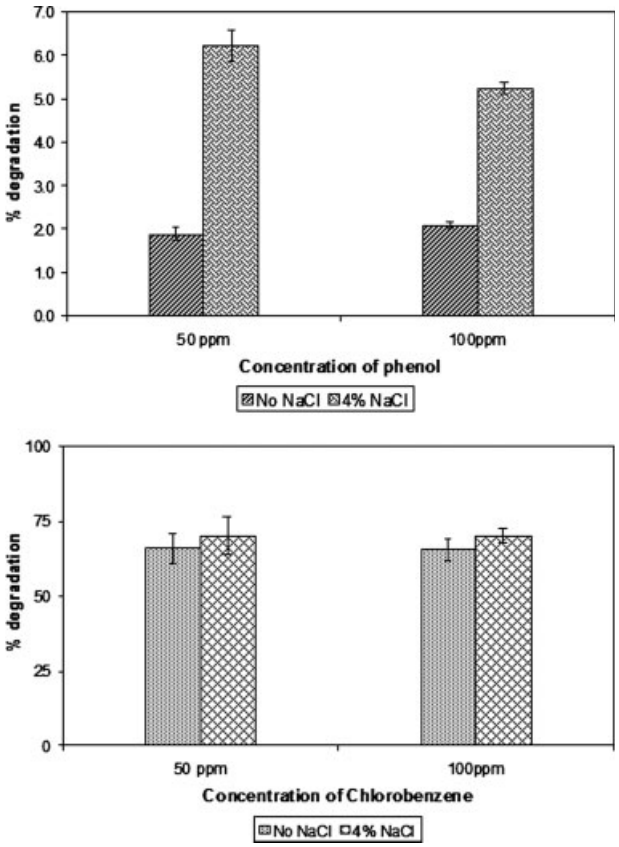

Figure 2. Experimental results on degradation of phenol and chlorobenzene under various reaction conditions.

Results and Discussion

The sonochemical degradation of pollutant occurs by two mechanisms, viz. pyrolysis in the cavitation bubble and hydroxylation (i.e. reaction with $OH^{\bullet}$ radicals generated by cavitation bubbles) in the bulk liquid medium. The principal factor that decides the contribution of the pyrolysis pathway is the diffusive flux of the pollutant molecules across bubble-bulk interface. The higher this flux, the higher the evaporation and the subsequent entrapment of the pollutant molecules in the bubble, which undergo thermal decomposition (pyrolysis) at the extreme conditions generated at the transient bubble collapse. The diffusive flux, as given by Eq. 5, depends on the partial pressure of the pollutant at the bubble-bulk interface, which in turn depends on the concentration of the pollutant in the interfacial region.

The principal factors that decide the contribution of the hydroxylation pathway are the rate of radical generation by the cavitation bubbles and the probability of interaction between the radicals and pollutant molecules. The extent of radical generation by the cavitation bubbles depends on amount of vapor (both water and pollutant) molecules trapped in the bubble at the collapse and the temperature reached during collapse. The radicals generated in the bubble mix with the bulk liquid medium with the fragmentation of the bubble during transient collapse. As the radical species are extremely reactive and unstable, they do not diffuse away significantly from the location of collapse of the bubble. Thus, significant fraction of the radical induced degradation (or hydroxylation) reaction occurs in a thin shell of liquid surrounding the cavitation bubble.[21,40,81–83] Obviously, the higher the concentration of pollutant molecules in this shell, the higher the probability of interaction between pollutant molecule and radical species and the higher the degradation. It needs to be mentioned that some hydroxylation reaction leading to degradation of the pollutant also occurs in the bulk medium. Rise in the bulk concentration of the pollutant increases the probability of the interaction between radical and pollutant in the bulk medium. Briefly, concentration of pollutant in the bubble-bulk interfacial region influences contribution of both pyrolysis and hydroxylation pathway to the degradation of pollutants. With this prelude, we present the results of experiments and simulations and try to establish the link between them.

Results for the degradation of phenol and chlorobenzene with different experimental conditions are shown in Figure 2. Certain trends in the experimental results are observed as follows: (1) the absolute amount of pollutant degraded in 90 min of sonication, in case of both phenol and chlorobenzene, increases with initial concentration of the pollutant—with all other conditions remaining the same; (2) with addition of 4% w/v NaCl, the extent of degradation for phenol rises ~threefold, while salt addition has negligible enhancement effect on the degradation of chlorobenzene; (3) other experimental conditions remaining the same, the degradation of chlorobenzene is one order of magnitude higher than the degradation of phenol.

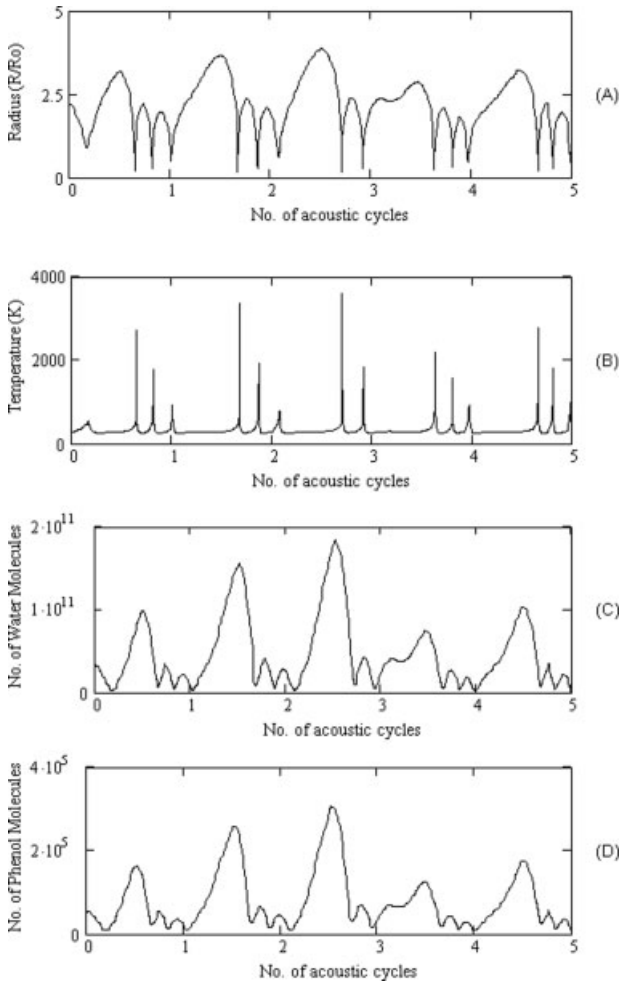

Figure 3. Simulation of the radial motion of 10-μm air bubble in 50 ppm phenol solution with 4% w/v NaCl.

Time variation of (A) Normalized bubble radius (R/R_0); (B) Temperature in the bubble; (C) Number of water molecules in the bubble; (D) Number of phenol molecules in the bubble.

Illustrative simulations of the radial motion of air bubbles in 50 ppm solution of phenol (with 4% w/v salt) and 100 ppm solution of chlorobenzene are shown in Figures 3 and 4, respectively. The summary of the entire simulation results is given in Table 3. This table lists the collapse conditions (i.e. the number of water and pollutant molecules trapped and the temperature peak reached in the bubble at transient collapse) along with equilibrium composition of various species that result out of dissociation of water and pollutant molecules trapped in the bubble. Some distinct trends observed in the simulation results are as follows: (1) the extent of entrapment of phenol molecules in the cavitation bubble is at least two orders of magnitude smaller than the chlorobenzene molecules; (2) with initial concentration increased from 50 to 100 ppm, the entrapment of phenol molecules in the bubble rises threefold, while the entrapment of chlorobenzene molecules remains practically unchanged. Moreover, with addition of 4% w/v salt to the solution, the entrapment of phenol in the bubble again rises by ~threefold whereas entrapment of chlorobenzene molecule shows a slight (~10%) increase. These trends can be explained as follows:

(1) Vapor pressure of phenol at the temperature of experiment (25°C) is 46 Pa while that of chlorobenzene is 1598 Pa. Because of the difference of two orders of magnitude in vapor pressure, the diffusive flux and entrapment of chlorobenzene molecules is far higher than phenol.

(2) The diffusive flux of pollutant molecules depends on the partial pressure of pollutant at bubble-bulk interface, which in turn depends on the concentration or mole fraction of the pollutant in the bulk liquid at the interface. As mentioned earlier, this mole fraction is given as: $x_{pR} = x_p K_{\text{interface-bulk}}$. Thus, a rise in either x_p (overall mole fraction of pollutant) or $K_{\text{interface-bulk}}$ (interfacial partition coefficient, which increases with salt addition) would raise the partial pressure of pollutant. However, the maximum limit to x_{pR} is decided by the solubility of pollutant. As seen from Table 1, in case of chlorobenzene, the partition coefficients are high while solubility is quite small (0.5 g/l), due to its hydrophobic nature. As a result, the

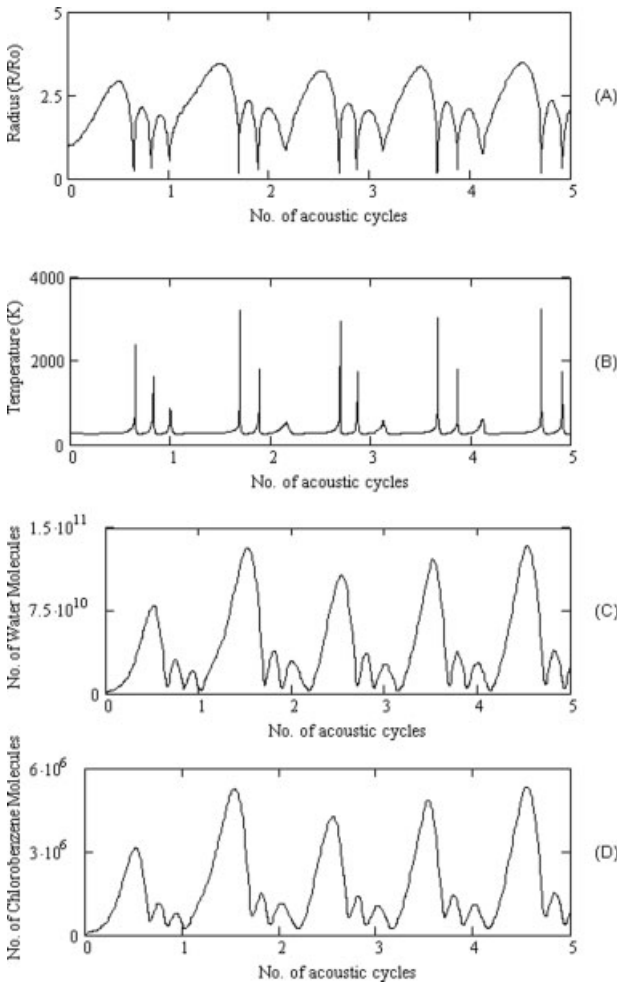

Figure 4. Simulation of the radial motion of 10-μm air bubble in 100 ppm chlorobenzene solution.

Time variation of (A) Normalized bubble radius (R/R_0); (B) Temperature in the bubble; (C) Number of water molecules in the bubble; (D) Number of chlorobenzene molecules in the bubble.

Table 3. (A) Simulation Results for the Phenol Solution and (B) Simulation Results for the Chlorobenzene Solution

Species	Parameters for Simulation: 50 ppm solution	50 ppm solution with 4% w/v NaCl	100 ppm solution	100 ppm solution with 4% w/v NaCl
Simulation Results for the Phenol Solution				
	Conditions at the first compression of the bubble			
	T_{max} = 2926 K N_{ph} = 8907 N_w = 9.25E+09	T_{max} = 2716 K N_{ph} = 26300 N_w = 7.41E+09	T_{max} = 2991 K N_{ph} = 20150 N_w = 1.06E+10	T_{max} = 2578 K N_{ph} = 49500 N_w = 7.13E+09
Equilibrium composition of different radical species in the bubble at collapse (mole fraction)				
O_2	8.644E-01	8.030E-01	8.784E-01	7.727E-01
H_2O	1.214E-01	1.866E-01	1.062E-01	2.194E-01
OH	1.090E-02	8.492E-03	1.158E-02	6.512E-03
O	1.862E-03	9.104E-04	2.261E-03	6.619E-04
HOO	1.202E-03	8.849E-04	1.300E-03	5.345E-04
H_2	1.051E-04	8.600E-05	1.095E-04	6.226E-05
H_2O_2	7.164E-05	6.611E-05	7.245E-05	5.387E-05
H	2.945E-05	1.474E-05	3.551E-05	9.292E-06
O_3	2.913E-05	1.428E-05	3.535E-05	8.672E-06
CO_2	1.863E-06	5.117E-06	4.278E-06	8.007E-06
CO	1.136E-08	1.555E-08	3.161E-08	1.650E-08
Simulation Results for the Chlorobenzene Solution				
	Conditions at the first compression of the bubble			
	T_{max} = 2383 K N_{cb} = 8.1E+05 N_w = 1.0502E+10	T_{max} = 2753 K N_{cb} = 9.412E+05 N_w = 1.18E+10	T_{max} = 2383 K N_{cb} = 8.1E+05 N_w = 1.0502E+10	T_{max} = 2753 K N_{cb} = 9.412E+05 N_w = 1.18E+10
Equilibrium composition of different radical species in the bubble at collapse (mole fraction)				
O_2	6.994E-01	8.188E-01	6.994E-01	8.188E-01
H_2O	2.955E-01	1.700E-01	2.955E-01	1.700E-01
OH	4.262E-03	8.826E-03	4.262E-03	8.826E-03
O	2.207E-04	1.037E-03	2.207E-04	1.037E-03
HOO	4.127E-04	9.384E-04	4.127E-04	9.384E-04
CO_2	1.375E-04	1.817E-04	1.375E-04	1.817E-04
H_2	3.879E-05	8.732E-05	3.879E-05	8.732E-05
H_2O_2	3.963E-05	6.695E-05	3.963E-05	6.695E-05
HCl	2.113E-05	2.540E-05	2.113E-05	2.540E-05
O_3	3.702E-06	1.658E-05	3.702E-06	1.658E-05
H	3.049E-06	1.647E-05	3.049E-06	1.647E-05
Cl	1.182E-06	3.306E-06	1.182E-06	3.306E-06
ClO	3.504E-07	1.163E-06	3.504E-07	1.163E-06
CO	1.035E-07	6.230E-07	1.035E-07	6.230E-07
HOCl	2.675E-07	5.066E-07	2.675E-07	5.066E-07
ClO_2	1.233E-09	6.043E-09	1.233E-09	6.043E-09
Cl_2	1.972E-10	4.655E-10	1.972E-10	4.655E-10

In the equilibrium composition, the number format is as follows: 2.075E-07 should be read as: 2.075×10^{-7}. Species having equilibrium mole fraction less than 10^{-10} have been ignored. Species with Nitrogen as a constituent element have been ignored, as they are found in traces and contribute little in the degradation reaction. Notations: T_{max} = Temperature in the bubble at the instance of first compression; N_W = water molecules trapped in the bubble at the instance of first compression; N_{ph} = phenol molecules trapped in the bubble during transient collapse; N_{cb} = chlorobenzene molecules trapped in the bubble during transient collapse.

interfacial region always remains saturated with chlorobenzene for all experimental conditions. Thus, the diffusive flux and entrapment of chlorobenzene remains practically unchanged irrespective of initial concentration and salt addition. In case of phenol, however, partition coefficients are relatively small due to its hydrophilic nature and the solubility is much higher (8 g/l). Therefore, the liquid in the interfacial region is considerably unsaturated. Increasing the bulk concentration or salt addition to the solution causes a net rise in the interfacial concentration of phenol, which raises its partial pressure. This results in an augmentation in the diffusive flux and the entrapment of phenol.

An immediate conclusion, which can be drawn from the results presented above, is that principal contribution to the sonochemical degradation of chlorobenzene is through pyrolysis route, while the principal contribution to the sonochemical degradation of phenol is through the hydroxylation route. This conclusion is further corroborated by the composition of various species generated in the bubble during transient collapse. As mentioned earlier, some of the intermediate species observed during sonochemical degradation of chlorobenzene comprise of HCl, HOCl, and $Cl^{\bullet}$. The simulation results for the radial bubble motion in chlorobenzene solution indeed show formation of these species during transient collapse of the bubble. On the other hand, the amount of phenol molecule entrapment in the bubble is quite small, and hence, the composition of the bubble contents at the transient collapse is dominated by radical species generated out of dissociation of water molecules such as $OH^{\bullet}$, $H^{\bullet}$, and $HOO^{\bullet}$. These species react with the phenol molecules present in the bubble-bulk interfacial region forming hydroxylated products such as hydroquinone and catechol, which have been observed as degradation intermediates, as noted earlier.

The overall degradation of both phenol and chlorobenzene increases with bulk concentration. Rise in bulk concentration influences both the pathways of degradation, i.e. pyrolysis and hydroxylation, to certain extent. Simulation results help us determine this extent for the two pollutants. As far as chlorobenzene is concerned the bubble-bulk interface is always saturated and increasing bulk concentration does not make any change. Hence, the diffusive flux and entrapment of chlorobenzene molecules remains practically unaltered with changes in bulk concentration. Moreover, the degree of hydroxylation reaction occurring in the interfacial region also does not change, as the pollutant concentration in this region is already at its maximum. With this, the rise in the extent of degradation is clearly attributed to larger degradation (mostly by hydroxylation) occurring in the bulk liquid, due to higher probability of interaction between radicals and pollutant molecules. For phenol, the mechanism is different. In this case, the liquid at the interfacial region is considerably unsaturated. With rise in bulk concentration, the concentration in the interfacial region also increases. This has two evident consequences: rise in the diffusive flux and entrapment of phenol molecules in the bubble, and secondly, increase in the probability of radical-pollutant interaction, which increases the degree of hydroxylation region occurring in the interfacial region.

The difference in the extent of degradation of phenol and chlorobenzene under similar conditions can be explained on the basis of simulation results. The entrapment of chlorobenzene molecules in the bubble is quite high. These molecules undergo complete degradation (or mineralization) at the extremes of temperature and pressure generated during transient bubble collapse. As a result, the degradation of chlorobenzene is rapid, with more than 60% of pollutant degraded in 90 min. Degradation of phenol occurs outside the bubble. Because of rather dilute solution used in the experiments, the probability of interaction of phenol molecules with radical species is relatively low. Hence, not all of the radical species generated by the bubble undergo reaction with phenol. Most of the species mere recombine to yield O_2, H_2O_2, and H_2O without inducing any degradation reaction. Accordingly, the extent of degradation is slow.

Assessment of the experimental and simulation results also explains the effect of salt addition on the degradation rate of the two pollutants. As stated earlier, the addition of salt increases the ionic strength of the solution that enhances the hydrophobic repulsive interactions between aqueous phase and pollutant, which drives the pollutant molecules towards bubble-bulk interface. Therefore, the concentration of the pollutant in the bubble-bulk interfacial region increases. This phenomenon has two consequences that contribute towards the enhancement of degradation. Firstly, the partial pressure of the pollutant at the interface increases. This results in rise of the diffusive flux and entrapment of pollutant molecules in the bubble. Thus, the contribution of the pyrolysis pathway to the degradation increases. Secondly, the probability of interaction between radical and pollutant molecule in the interfacial region also increases, which increases the extent of hydroxylation reaction occurring in this region. However, the magnitude of salt induced enhancement is different for the two pollutants. For chlorobenzene, as the interfacial region is always saturated, neither the entrapment of molecules nor the interactions with radicals change with salt addition. As a result, the extent of degradation practically remains constant. On the other hand, entrapment of phenol molecules rises by ~threefold with salt addition. Therefore, contribution of the pyrolysis route to phenol degradation boosts drastically. Secondly, the net production of the $OH^{\bullet}$ radicals per bubble remains practically constant with salt addition to the solution but the net utility of these radicals for the degradation of pollutant increases. Higher concentration of phenol molecules near bubble-bulk interface also raises the probability of interaction with radical species, which further adds to the degradation via hydroxylation route. On the whole, salt addition causes a sharp rise in the overall degradation of phenol in 90 min of sonication.

Conclusion

In this article, we have tried to explain the physical or mechanistic features of the sonochemical degradation of volatile and nonvolatile organic pollutants. With experiments using chlorobenzene and phenol as model pollutants and a mathematical model for radial motion of cavitation bubbles, we have explored some remarkable mechanistic features of the sonochemical degradation of these pollutants. Our results reveal that thermal decomposition or pyrolysis in the cavitation bubble is the predominant mechanism of degradation of volatile pollutants while hydroxylation in the bulk medium is the principal pathway for the degradation of nonvolatile pollutants. These results are in accordance with the previous literature in which intermediates and products of the degradation reaction have been used to determine the mechanism of sonochemical degradation. We have also investigated changes in the extent of degradation with variation of some experimental parameters such as bulk concentration of pollutant and salt addition to the solution of pollutant. Concurrent evaluation of experimental and simulation results reveals that these parameters influence both the pathways of degradation. However, the magnitude of this influence is different for phenol and chlorobenzene, which is attributed to the different nature (hydrophobic and hydrophilic) of the pollutant. To conclude, this article provides a framework for deducing the mechanistic features of the sonochemical degradation of organic pollutants, knowledge of which is of paramount importance in designing large-scale processes for ultrasound-aided wastewater treatment.

Acknowledgments

VSM thank DST, Government of India for the funding of the project under Fast Track Scheme for Young Scientists.

Literature Cited

1. Bauer R, Fallmann H. The photo-Fenton oxidation—a cheap and efficient wastewater treatment method. *Res Chem Intermed*. 1997; 23:341–354.
2. Mantzavinos D, Hellenbrand R, Livingston AG, Metcalf IS. Reaction mechanisms and kinetics of chemical pretreatment of bioresistant organic molecules by wet air oxidation. *Water Sci Technol*. 1997;35:119–127.
3. Feigelson L, Muszkat L, Bir L, Muszkat KA. Dye photo-enhancement of TiO_2-photocatalyzed degradation of organic pollutants: the organobromine herbicide bromacil. *Water Sci Technol*. 2000;42:275–279.

4. Hua I, Hoffmann MR. Kinetics and mechanism of sonolytic degradation of CCl_4: Intermediates and byproducts. *Environ Sci Tech*. 1996;30:864–871.
5. Colussi A, Hung H, Hoffmann MR. Sonochemical degradation rates of volatile solutes. *J Phys Chem A*. 1999;103:2696–2699.
6. Petrier C, Francony A. Ultrasonic waste-water treatment: incidence of ultrasonic frequency on the rate of phenol and carbon tetrachloride degradation. *Ultrason Sonochem*. 1997;4:295–300.
7. Hung H, Hoffmann MR. Kinetics and mechanism of sonolytic degradation of chlorinated hydrocarbons: frequency effects. *J Phys Chem A*. 1999;103:2734–2739.
8. Lin J, Ma Y. Magnitude of effect of reaction parameters on 2-chlorophenol decomposition by ultrasonic process. *J Hazard Mater B*. 1999;66:291–305.
9. Peller J, Wiest O, Kamat P. Sonolysis of 2,4-dichlorophenoxyacetic acid in aqueous solution. Evidence for OH radical mediated degradation. *J Phys Chem A*. 2001;105:3176–3181.
10. Bhatnagar A, Cheung H. Sonochemical destruction of chlorinated C_1 and C_2 volatile organic compounds in dilute aqueous solution. *Environ Sci Technol*. 1994;28:1481–1486.
11. Barbier P, Petrier C. Study at 20 kHz and 500 kHz of the ultrasound-ozone advanced oxidation system: 4-nitrophenol degradation. *J Adv Oxidation Technol*. 1996;1:154–159.
12. Beckett M, Hua I. Elucidation of the 1,4-dioxane decomposition pathway at discrete ultrasonic frequencies. *Environ Sci Technol*. 2000;34:3944–3953.
13. Kotronarou A, Mills G, Hoffmann MR. Decomposition of parathion in aqueous solution by ultrasonic irradiation. *Environ Sci Technol*. 1992;26:1460–1462.
14. Kotronarou A, Mills G, Hoffmann MR. Ultrasonic irradiation of p-nitrophenol in aqueous solution. *J Phys Chem*. 1991;95:3630–3638.
15. Okouchi S, Nojima O, Arai T. Cavitation induced degradation of phenol by ultrasound. *Water Sci Technol*. 1992;26:2053–2056.
16. Kang J, Hung H, Lin A, Hoffmann MR. Sonolytic destruction of methyl tert-butyl ether by ultrasonic irradiation: The role of O_3, H_2O_2, frequency, and power density. *Environ Sci Tech*. 1999;33:3199–3205.
17. Weavers LK, Malmstadt N, Hoffmann MR. Kinetics and mechanism of pentachlorophenol degradation by sonication, ozonation and sonolytic ozonation. *Environ Sci Tech*. 2000;34:1280–1285.
18. Weavers LK, Ling FH, Hoffmann MR. Aromatic compound degradation in water by combination of sonolysis and ozonolysis. *Environ Sci Tech*. 1998;32:2727–2733.
19. Vinodgopal K, Peller J. Hydroxyl radical-mediated advanced oxidation processes for textile dyes: a comparison of the radiolytic and sonolytic degradation of the monoazo dye acid orange 7. *Res Chem Intermed*. 2003;29:307–316.
20. Joseph J, Destaillats H, Hung H, Hoffmann MR. The sonochemical degradation of azobenzene and related azo dyes: rate enhancements via Fenton's reactions. *J Phys Chem A*. 2000;104:301–307.
21. Suslick KS. Sonochemistry. *Science*. 1990;247:1439–1445.
22. Flint EB, Suslick KS. The temperature of cavitation. *Science*. 1991; 253:1397–1399.
23. Hart EJ, Henglein A. Free radical and free atom reactions in the sonolysis of aqueous iodide and formate solutions. *J Phys Chem*. 1985;89:4342–4347.
24. Hart EJ, Henglein A. Sonochemistry of aqueous solutions: hydrogen-oxygen combustion in cavitation bubbles. *J Phys Chem*. 1987;91:3654–3656.
25. Henglein A. The acceleration of chemical reaction induced by ultrasound in solutions of oxygen noble gas mixtures. *Naturwissenschaften*. 1956;43:277.
26. Brenner M, Hilgenfeldt S, Lohse D. Single-bubble sonoluminescence. *Rev Mod Phys*. 2002;74:425–484.
27. Colussi A, Weavers LK, Hoffmann MR. Chemical bubble dynamics and quantitative sonochemistry. *J Phys Chem A*. 1998;35:6927–6934.
28. Weavers LK, Hoffmann MR. Sonolytic decomposition of ozone in aqueous solutions: mass transfer effects. *Environ Sci Technol*. 1998; 32:3941–3947.
29. Lesko TM. Chemical Effects of Acoustic Cavitation. Ph.D. Thesis, Pasadena: California Institute of Technology, 2004.
30. Storey BD, Szeri AJ. Water vapor, sonoluminescence and sonochemistry. *Proc R Soc Lond Ser A*. 2000;456:1685–1709.
31. Hua I, Hochemer RH, Hoffmann MR. Sonochemical degradation of p-Nitrophenol in a parallel plate near field acoustic processor. *Environ Sci Technol*. 1995;29:2790–2796.
32. Berlan J, Trabelsi F, Delmas H, Wilhelm AM, Petrignani JF. Oxidative degradation of phenol in aqueous media using ultrasound. *Ultrason Sonochem*. 1994;1:S97–S102.
33. Gogate PR, Mujumdar S, Thampi J, Wilhelm AM, Pandit AB. Destruction of phenol using sonochemical reactors: scale-up aspects and comparison of novel configuration with conventional reactors. *Sep Purif Technol*. 2004;34:25–34.
34. Petrier C, Lamy MF, Francony A, Benahcene A, David B, Renaudin V, Gondrexon N. Sonochemical degradation of phenol in dilute aqueous solutions: comparison of the reaction rates at 20 and 487 kHz. *J Phys Chem*. 1994;98:10514–10520.
35. Entezari MH, Petrier C. A Combination of ultrasound and oxidative enzyme: sonoenzyme degradation of phenols in a mixture. *Ultrason Sonochem*. 2005;12:283–288.
36. Entezari MH, Petrier C, Devidal P. Sonochemical degradation of phenol: a comparison of classical equipment with a new cylindrical reactor. *Ultrason Sonochem*. 2003;10:103–108.
37. Mahamuni NN, Pandit AB. Effect of additives on ultrasonic degradation of phenol. *Ultrason Sonochem*. 2006;13:165–174.
38. Trabelsi F, Ait-Lyazidi H, Ratsimba B, Wilhelm AM, Delmas H, Fabre PL, Berlan J. Oxidation of phenol in wastewater by sonochemistry. *Chem Eng Sci*. 1996;51:1857–1865.
39. Chen Y, Smirniotis P. Enhancement of photocatalytic degradation of phenol and chlorophenols with ultrasound. *Ind Eng Chem Res*. 2002;41:5958–5965.
40. Seymour J, Gupta RB. Oxidation of aqueous pollutants using ultrasound: salt induced enhancement. *Ind Eng Chem Res*. 1997;36: 3453–3457.
41. Drijvers D, Langenhove HV, Vervaet K. Sonolysis of chlorobenzene in aqueous solution: organic intermediates. *Ultrason Sonochem*. 1998; 5:13–19.
42. Price GJ, Matthias P, Lenz EJ. The use of high power ultrasound for the destruction of aromatic compounds in aqueous solutions. *Trans Inst Chem Engrs*. 1994;72:27–31.
43. Drijvers D, Langenhove HV, Herrygers V. Sonolysis of fluoro-, chloro-, bromo- and iodobenzene: a comparative study. *Ultrason Sonochem*. 2000;7:87–95.
44. Drijvers D, Langenhove HV, Beckers M. Decomposition of phenol and trichloroethylene by the US/H2O2/CuO process. *Water Res*. 1999;33:1187–1194.
45. Dewulf J, Langenhove HV, Visscher AD, Sabbe S. Ultrasonic degradation of trichloroethylene and chlorobenzene at micromolar concentration: kinetics and modeling. *Ultrason Sonochem*. 2001;8:143–150.
46. Kruus P, Burk RC, Entezari MH, Otson R. Sonication of aqueous solutions of chlorobenzene. *Ultrason Sonochem*. 1997;4:229–233.
47. Okuno H, Yim B, Mizukoshi Y, Nagata Y, Maeda Y. Sonolytic degradation of hazardous organic compounds in aqueous solutions. *Ultrason Sonochem*. 2000;7:261–264.
48. Petrier C, Combet E, Mason T. Oxygen induced concurrent ultrasonic degradation of volatile and non-volatile aromatic compounds. *Ultrason Sonochem*. 2007;14:117–121.
49. Stavarache C, Yim B, Vinatoru M, Maeda Y. Sonolysis of chlorobenzene in Fenton type aqueous systems. *Ultrason Sonochem*. 2002; 9:291–296.
50. Stavarache C, Vinatoru M, Nishimura R, Maeda Y. Short time Sonolysis of chlorobenzene in presence of Pd(II) salts and Pd(0). *Ultrason Sonochem*. 2004;11:429–434.
51. Yi J, Petrier C, Waite D. Kinetics and mechanism of ultrasonic degradation of volatile chlorinated aromatics in aqueous solutions. *Ultrason Sonochem*. 2002;9:317–323.
52. Sivasankar T, Paunikar AW, Moholkar VS. Mechanistic approach to enhancement of the yield of a sonochemical reaction. *AIChE J*. 2007;53:1132–1143.
53. Gogate PR, Pandit AB. A review of imperative technologies for wastewater treatment I: oxidation technologies at ambient conditions. *Adv Environ Res*. 2004;8:501–551.
54. Prasad Naidu DV, Rajan R, Kumar R, Gandhi KS, Arakeri VH, Chandrasekaran S. Modeling of a batch sonochemical reactor. *Chem Eng Sci*. 1994;49:877–888.
55. Kamath V, Prosperetti A, Egolfopoulos FN. A Theoretical Study of Sonoluminescence. *J Acoust Soc Am*. 1993;94:248–260.
56. Gong C, Hart DP. Ultrasound induced cavitation and sonochemical yields. *J Acoust Soc Am*. 1998;104:2675–2682.

57. Sochard S, Wilhelm AM, Delmas H. Modeling of free radicals production in a collapsing gas-vapor bubble. *Ultrason Sonochem.* 1997;4: 77–84.
58. Moss WC, Young DA, Harte JA, Levalin JL, Rozsnyai BF, Zimmerman GB, Zimmerman IH. Computed optical emissions from sonoluminescing bubbles. *Phys Rev E*. 1999;59:2986–2992.
59. Colussi AJ; Hoffmann MR. Vapor supersaturation in collapsing bubbles. Relevance to mechanisms of sonochemistry and sonoluminescence. *J Phys Chem A*. 1999;103:11336–11339.
60. Yasui K. Alternative model for single-bubble sonoluminescence. *Phys Rev E*. 1997;56:6750–6760.
61. Yasui K. Chemical reactions in a sonoluminescing bubble. *J Phys Soc Jpn*. 1997;66:2911–2920.
62. Toegel R, Gompf B, Pecha R, Lohse D. Does water vapor prevent upscaling sonoluminescence? *Phys Rev Lett*. 2000;85:3165–3168.
63. Toegel R, Lohse D. Phase diagrams for sonoluminescing bubbles: a comparison between experiment and theory. *J Chem Phys*. 2003; 118:1863–1875.
64. Ilyichev VI, Koretz VL, Melnokov NP. Spectral characteristics of acoustic cavitation. *Ultrasonics*. 1989;27:357–361.
65. Brennen CE. *Cavitation and Bubble Dynamics*. Oxford: Oxford University Press, 1995.
66. Prosperetti A, Lezzi A. Bubble dynamics in a compressible liquid. Part 1. First order theory. *J Fluid Mech.* 1986;168:457–477.
67. Hilgenfeldt S, Lohse D, Brenner MP. Phase diagrams for sonoluminescing bubbles. *Phys Fluids*. 1996;8:2808–2826.
68. Joos P, Serrien G. Adsorption kinetics of lower alkanols at the air/water interface: effect of structure makes and structure breakers. *J Colloid Interfacial Sci*. 1989;127:97–103.
69. Price GJ, Ashok kumar M, Grieser F. Sonoluminescence quenching of organic compounds in aqueous solution: frequency effects and implications for sonochemistry. *J Am Chem Soc*. 2004;126:2755–2762.
70. Bapat PS, Gogate PR, Pandit AB. Theoretical analysis of sonochemical degradation of phenol and its chloro-derivatives. *Ultrason Sonochem*. 2008;15:564–570.
71. Adamson AW, Gast AP. *Physical Chemistry of Surfaces*. New York: Wiley, 1997.
72. NIST Data Gateway, Chemistry Webbook, 2001. Available at http://webbook.nist.gov/chemistry.
73. Al-Shayji KA. *Modeling, simulation and optimization of large scale commercial desalination plants*. Ph.D. Dissertation, Virginia Polytechnique Institute and State University, Blacksburg, April 1998.
74. Krishnan SJ, Dwivedi P, Moholkar VS. Numerical investigation into the chemistry induced by hydrodynamic cavitation. *Ind Eng Chem Res*. 2006;45:1493–1504.
75. Kumar KS, Moholkar VS. Conceptual design of a novel hydrodynamic cavitation reactor. *Chem Eng Sci*. 2007;62:2698–2711.
76. Hirschfelder JO, Curtiss CF, Bird RB. *Molecular Theory of Gases and Liquids*. New York: Wiley, 1954.
77. Bird RB, Stewart WE, Lightfoot EN. *Transport phenomena*, 2nd ed. New York: Wiley, 2001.
78. Odishaw H, Condon EU. *Handbook of Physics*. New York: McGraw-Hill, 1958.
79. Press WH, Teukolsky SA, Flannery BP, Vetterling WT. *Numerical Recipes*, 2nd ed. New York: Cambridge University Press, 1992.
80. Eriksson G. Thermodynamic studies of high temperature equilibria-XII: SOLGAMIX, a computer program for calculation of equilibrium composition in multiphase systems. *Chem Scr*. 1975;8:100–103.
81. Suslick KS. The chemical effects of ultrasound. *Sci Am*. 1989; 260:80–86.
82. Riesz P, Berdahl D, Christman CL. Free radical generation by ultrasound in aqueous and non-aqueous solutions. *Environ Health Perspect*. 1985;64:233–252.
83. Hoffmann MR, Hua I, Hochemer R. Application of ultrasonic irradiation for the degradation of chemical contaminants in water. *Ultrason Sonochem*. 1996;3:163–172.

Manuscript received July 29, 2007, revision received Jan. 9, 2008, and final revision received May 13, 2008.